Department of Ocean and Resources Engineering
School of Ocean and Earth Science and Technology

UNIVERSITY of HAWAI'I® MĀNOA

October 25, 2020

Leo Rustum J. Espia
Deputy Administrator and State Hazard Mitigation Officer
Guam Homeland Security and Office of Civil Defense
221-B Chalan Palasyo, Agana Heights
Guam 96910

RE: Progress Report "Tsunami Hazard Modeling and Mapping for Agat Marina, Guam"

Dear Mr. Espia,

Attached please find the above referenced report that summaries the background, methodology, and data products for Agat Marina. This submittal also includes a set of tsunami hazard maps in ArcGIS format. I will make arrangement with PacIOOS to place the model output on its online data server for public access (https://www.pacioos.hawaii.edu/metadata). If you need additional information, please contact me by phone at (808) 956-3485 or by email at cheung@hawaii.edu.

Yours truly,

Kwok Fai Cheung, PhD, PE
Professor and Graduate Chair

2450 Dole Street, Holmes 402, Honolulu, Hawai'i 96822
Telephone: 808.956.7572 Fax: 808.956.3498

Background

The National Tsunami Hazard Mitigation Program (NTHMP) is supporting state and regional efforts in developing tsunami hazard maps for the maritime communities. Guam Homeland Security began the effort with the University of Hawaii in November 2017. Stakeholder meetings with United States Coast Guard (USCG) District 14 Sector Guam, Port Authority of Guam, Guam Naval Base Emergency Management, Guam Waterworks Authority, and Guam Power Authority provided guidance in defining the data products. The USCG District 14 operating procedures call for evacuation of ships and shore personnel in a tsunami warning, when the predicted nearshore wave amplitude is over 1 m, but do not have provisions for tsunami advisories, which involve predicted near-shore amplitude of less than 1 m. Localized currents and drawdown might pose navigational hazards and damage ships and mooring systems despite low potential for inundation. The data products include offshore surge and current based on probable maximum tsunami scenarios as well as in-harbor hazard maps of surge, drawdown, and current for advisory-level tsunamis from potential source regions. The data products for Apra Harbor, Agana Bay, and Tumon Bay have been completed and delivered to Guam Homeland Security. This progress report summarizes the methodologies and data products for Agat Marina.

1. Tsunami Scenarios

A sensitivity analysis helps identify tsunami sources most critical to Guam for data product development. Gica et al. (2008) discretized the subduction zones of the Pacific into subfaults and compiled the fault parameters that can be implemented in the planar fault model of Okada (1985) to determine the seafloor deformation from earthquake rupture. We utilize NEOWAVE (Non-hydrostatic Evolution of Ocean Waves) to model tsunamis generated by hypothetical Mw 8.5 earthquakes at the individual subfaults. Figure 1 shows the computed wave amplitude at 500 m water depth off the west shore of Guam from the respective sources. The results indicate the Mariana, Nankai, Ryukyu, Philippine, New Guinea, and Manus subduction zones are potentially critical to Guam. Tsunamis from the New Britain, Solomon, and New Hebrides subduction zones, Tonga-Kermadec Trench, and the Americas in general have relatively minor effects. The wave amplitude from sources at the westernmost Aleutians is appreciable, but is probably overestimated as the relative plate motion is approaching trench parallel toward Kamchatka (Lay et al., 2017).

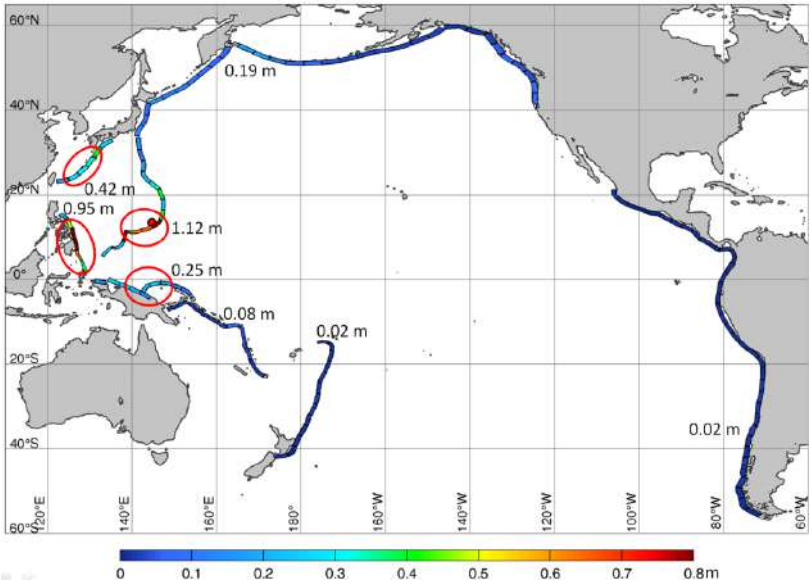

Figure 1. Sensitivity analysis of tsunami wave amplitude off the west shore of Guam from hypothetical Mw 8.5 earthquakes at subduction zones in the Pacific Ocean.

Table 1 summarizes the dip angles of the critical tsunami sources around Guam from Gica et al. (2008) and the convergence rate, coupling coefficient, and maximum magnitude from the Global Earthquake Model of Berryman et al. (2015). The potential tsunami threats can be categorized by source location or approaching direction. The Mariana subduction zone is nearest to Guam and a tsunami generated there has little time for warning and response. Such locally generated tsunamis are included in the modeling to provide data for planning purposes. The Nankai and Ryukyu sources belong to the same subduction zone. The former is considered for modeling because of its higher seismicity associated with stronger coupling and the larger, preferred maximum magnitude. Tsunamigenic earthquakes at Nankai Trough have recurrence intervals of 100 to 200 years during the last 1300 years (Ando, 1975). The presence of comprehensive records and measurements explains the narrow parameter ranges in the table. The plate boundary along the Philippine Trench represents tsunami sources from the west and the large dip angle make it effective in generating uplift. New Guinea and Manus belong to separate subduction zones, but the resulting tsunamis have similar impacts to Guam. The New Guinea subduction zone, which has higher seismicity, is selected as a representative tsunami source from the south.

Table 1. Seismicity of tsunami sources with potential impact to Guam

Tsunami Source		Dip (°)	Convergence Rate (mm/yr)	Coupling Coefficient (Preferred)	Maximum Magnitude (Preferred)
Local	Mariana	22	63	0.1 - 0.7 (0.20)	7.2 - 9.5 (8.3)
North	Nankai	13	50	0.8 - 1.0 (0.90)	8.5 - 8.9 (8.7)
	Ryukyu	17	96	0.1 - 0.7 (0.20)	8.0 - 9.1 (8.5)
West	Philippine	46	36	0.1 - 0.8 (0.25)	7.6 - 9.3 (8.5)
South	New Guinea	8	22	0.6 - 0.8 (0.70)	8.2 - 9.4 (8.8)
	Manus	15	9	0.3 - 0.7 (0.50)	7.5 - 9.5 (8.5)

We model tsunamis from each source over a moment magnitude range to cover advisory to warning-level tsunamis reaching Guam. The discretization from Gica et al. (2008) provides the fault geometries and parameters for the four selected subduction zones. The rupture area is determined from the moment magnitude using the scaling relation of Ye et al. (2016a, b), who analyzed 114 earthquakes of the circum-Pacific mega-thrusts with Mw ≥ 7.0 from 1990 to 2015. Their proposed width to length ratio of 0.2423 allows determination of the fault dimensions in the dip and strike directions. The rupture within each zone is aligned with the trench and positioned to give the most direct path of the resulting tsunamis to Guam as illustrated in Figure 2. If the rupture reaches the full width of the subduction zone, we extend the fault length to match the rupture area associated with the seismic moment. A typical value of 3×10^{10} N/m^2, consistent with Ye et al. (2016a, b), accounts for the rigidity in the computation of the average slip using the scaling relation of Kanamori (1997).

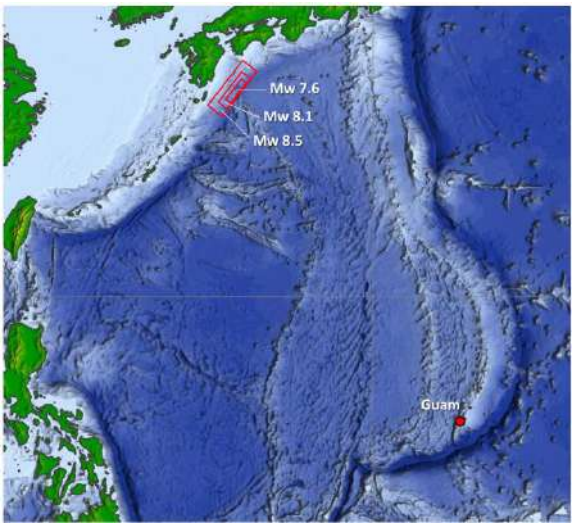

Figure 2. Illustration of rupture models at Nankai Trough.

Table 2. Source parameters as functions of earthquake magnitude

Mw	Area (km^2)	Length (km)	Width (km)	Up-dip slip (m)	Down-dip slip (m)
7.5	2239	96	23	4.2	2.1
7.6	2818	108	26	4.7	2.3
7.7	3548	121	29	5.3	2.6
7.8	4467	136	33	5.9	3.0
7.9	5623	152	37	6.7	3.3
8.0	7080	171	41	7.5	3.7
8.1	8912	192	46	8.4	4.2
8.2	11220	215	52	9.4	4.7
8.3	14125	241	58	10.5	5.3
8.4	17783	271	66	11.8	5.9
8.5	22387	300	75	13.3	6.6
8.6	28184	341	83	14.9	7.4
8.7	35481	383	93	16.7	8.3
8.8	44649	446	100	18.7	9.4

While the scaling relation of Kanamori (1977) provides the average slip for a given moment magnitude, recent tsunami hazard assessments for California and Hawaii have placed larger slip toward the trench to mimic the rupture of the 2011 Tohoku earthquake (e.g., Ross et al., 2013; Bai et al., 2018). Following the approach of Bai et al. (2018), we place twice the slip in the up-dip half of the rupture area to produce more energetic tsunamis for the same seismic moment. Table 2 lists the seismic source parameters as functions of moment magnitude for the earthquake scenarios at the Mariana, Nankai, Philippine, and New Guinea subduction zones. Although the source parameters only depend on the moment magnitude, the resulting tsunami is also influenced by the local tectonics and water depth.

2. Model Setup

We utilize NEOWAVE to model each tsunami from its source to Agat Marina. The staggered finite-difference model builds on the nonlinear shallow-water equations with a vertical velocity term to account for dispersive tsunami waves and a momentum conservation scheme to describe flow discontinuities (Yamazaki et al., 2009, 2011). These specialized features enable modeling of the vertical flow structure over steep volcanic slopes as well as tsunami bores and hydraulic jumps that might develop in the shallow-reef environment of the Mariana Islands. NEOWAVE has been validated with laboratory and field benchmarks for modeling of coastal currents and inundation by the National Tsunami Hazard Mitigation Program (Yamazaki et al., 2012; Bai et al., 2015).

Modeling of tsunami propagation and inundation requires a digital elevation model of increasing resolution from the open ocean to the coast. We utilize the General Bathymetry Chart of the Oceans (GEBCO) at 30 arcsec (~900 m) resolution for the open ocean and a blended, high-resolution dataset near Guam consisting of

- 2001 USACE SHOALS LiDAR bathymetry to 40 m depth at 4 m resolution

- 2011 University of Hawaii SOEST multibeam bathymetry to 3.5 km depth at 60 m resolution
- 2007 University of Hawaii SOEST multibeam bathymetry to 400 m depth at 5 m resolution
- 2007 USACE LiDAR topography at 0.5 m resolution for the entire island of Guam
- 2007 USACE LiDAR bathymetry at 4 m resolution (limited coverage)
- 2008 US Navy & NOAA multibeam bathymetry of Apra Harbor at 1 m resolution

The dataset is supplemented by digitization of NOAA charts at shallow reefs, aerial images from Google Earth, and information gathered during the field visits in August 2019. We use the *bare-earth* data, which excludes buildings and vegetation, in the digital elevation model to be consistent with the standard practice for tsunami inundation mapping.

Five levels of telescopic grids in spherical coordinates are needed to model the tsunami from each earthquake source with increasing resolution to Agat Marina. Figure 3 shows the layout of the computational grid systems. The nesting scheme includes two-way communications during the computation and does not require external transfer of data between grid layers. Each grid contains bathymetric features of a scale appropriate to the resolution and physical processes. A level-1 grid describes tsunami propagation from the Nankai source to Guam and a second level-1 grid, shifted to the south, caters to the Mariana, Philippine, and New Guinea sources. The 2-arcmin (~3700 m) resolution give rise to optimal dispersion properties for modeling of trans-oceanic tsunami propagation with NEOWAVE (Li and Cheung, 2019). The level-2 grid captures wave transformation along the Mariana Island chain at higher resolution of 24 arcsec (~720 m) and provides a transition to the 2.4-arcsec (~72 m) level-3 grid that can resolve the steep slopes and narrow shelves around Guam. The level-4 grid covers a segment of Agat shorelines with low-lying coastal plains. The 0.6 arcsec (~18 m) resolution adequately describes the nearshore reef systems as a transition to the level-5 grid at 0.15 arcsec (~4.5 m), which is needed to resolve the breakwater of Agat Marina and the flow in and out through a narrow section of the channel.

Pile-supported piers and bridges, which allow passage of the flow underneath, are often represented as terrain features in LiDAR topography. These structures were removed from the high-resolution computational grids, if their presence is expected to modify the surrounding flow in a substantial way, and the elevation was interpolated from neighboring grid points. A Manning coefficient of 0.035 describes the subgrid roughness of tropical island environments (Bretschneider et al., 1986), while a value of 0.025 is optimal in resolving currents in harbors (Bai et al., 2015). The Mean Higher High Water (MHHW) and the Mean Lower Low Water (MLLW) levels at the Apra Harbor tide gauge are 0.296 and 0.419 m above and below the mean sea level (MSL) (https://tidesandcurrents.noaa.gov). The MSL is used to represent an average condition in the development of the data products, which will be used primarily to support maritime operations during tsunami advisories.

3. Data Products

The computation covers 5 hours of elapsed time after arrival of each tsunami at Agat Marina. This allows development of multi-scale standing waves over Guam's insular slope and reef complex that contribute to energetic surges and currents commonly observed in tropical island environments during a tsunami (Roeber et al., 2010; Cheung et al., 2013). NEOWAVE produces a large volume of spatial and temporal data at various coverage and resolution for post-processing. This section provides samples of the data products from each tsunami source for

illustration. The ArcGIS data products, which are submitted together with this report, cover the full range of tsunami scenarios considered in this study. All surface elevations in this report reference the MSL.

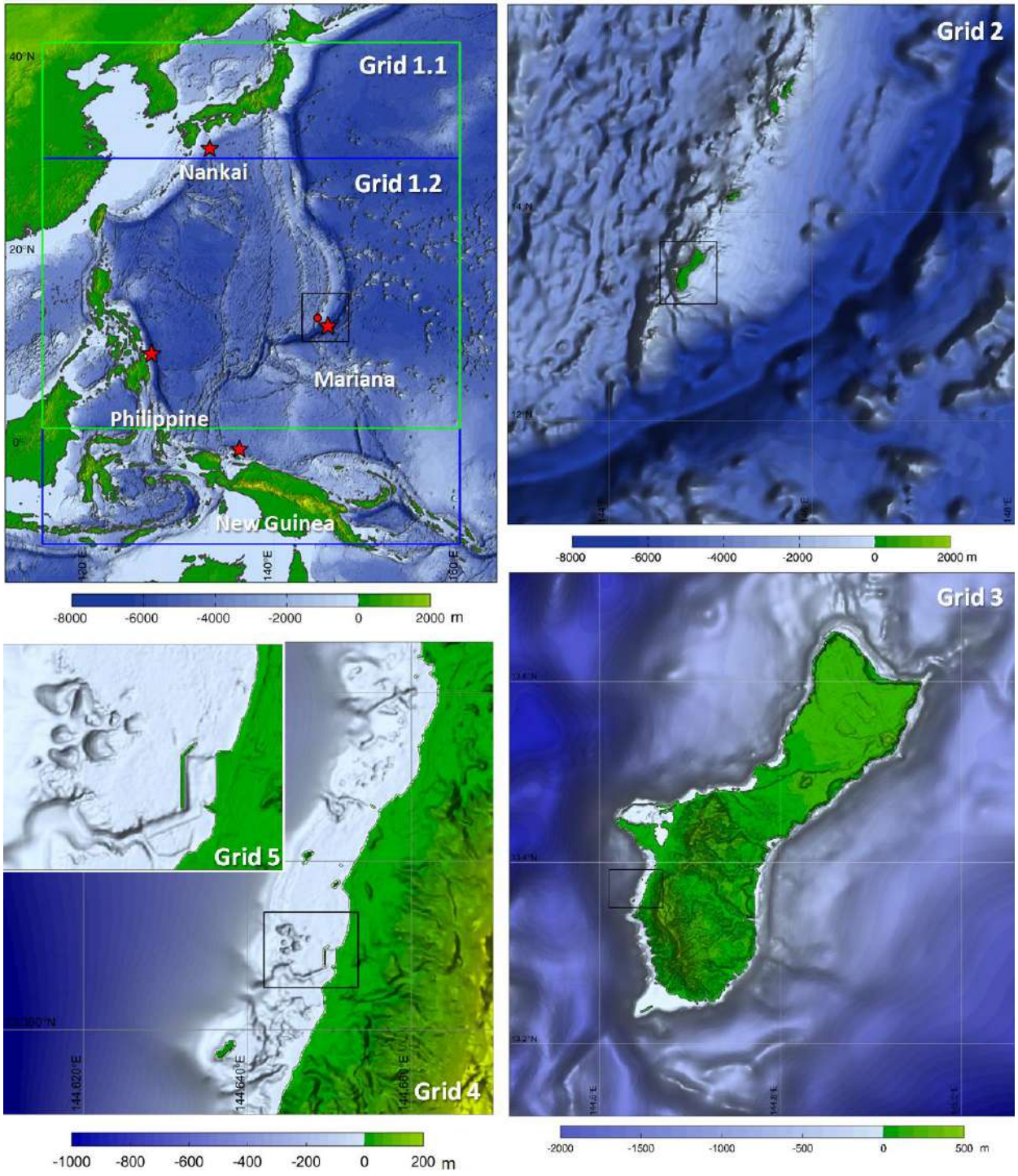

Figure 3. Layout of the five levels of computational grids. Red circle and stars identify Guam and tsunami sources within the level-1 grids. The topography and bathymetry references the MSL.

3.1 Tsunami Scenarios

The Mariana source is located immediately southeast of Guam and a tsunami generated there takes 10 min to reach the Agat shore. There is insufficient time to issue advisories or warning to the maritime communities and the model results are intended for planning and outreach purposes. Figure 4 shows the surge, drawdown, and current from tsunamis generated by Mw 7.6, 7.8, and 8.0 earthquakes to illustrate the progression of potential impacts. The Mw 7.6 event produces nearshore wave amplitude of just below 1 m with no major flooding except for the low-lying area of Nimitz Beach Park. However, damage to boats or moorings are likely from the drawdown of 1.1 m in the marina and the locally accelerated current to 4.2 m/s by the groin at the entrance. The short-period near-field tsunami produces significant build-up of the surge over the shallow reefs. The Mw 7.8 event shows overtopping of the breakwater and flooding inland of Highway 2. The overtopping reduces the drawdown during receding waves and arguments the outflow currents along the channel. The Mw 8.0 event produces extensive inundation along the shore and dangerous flow conditions across the reef system.

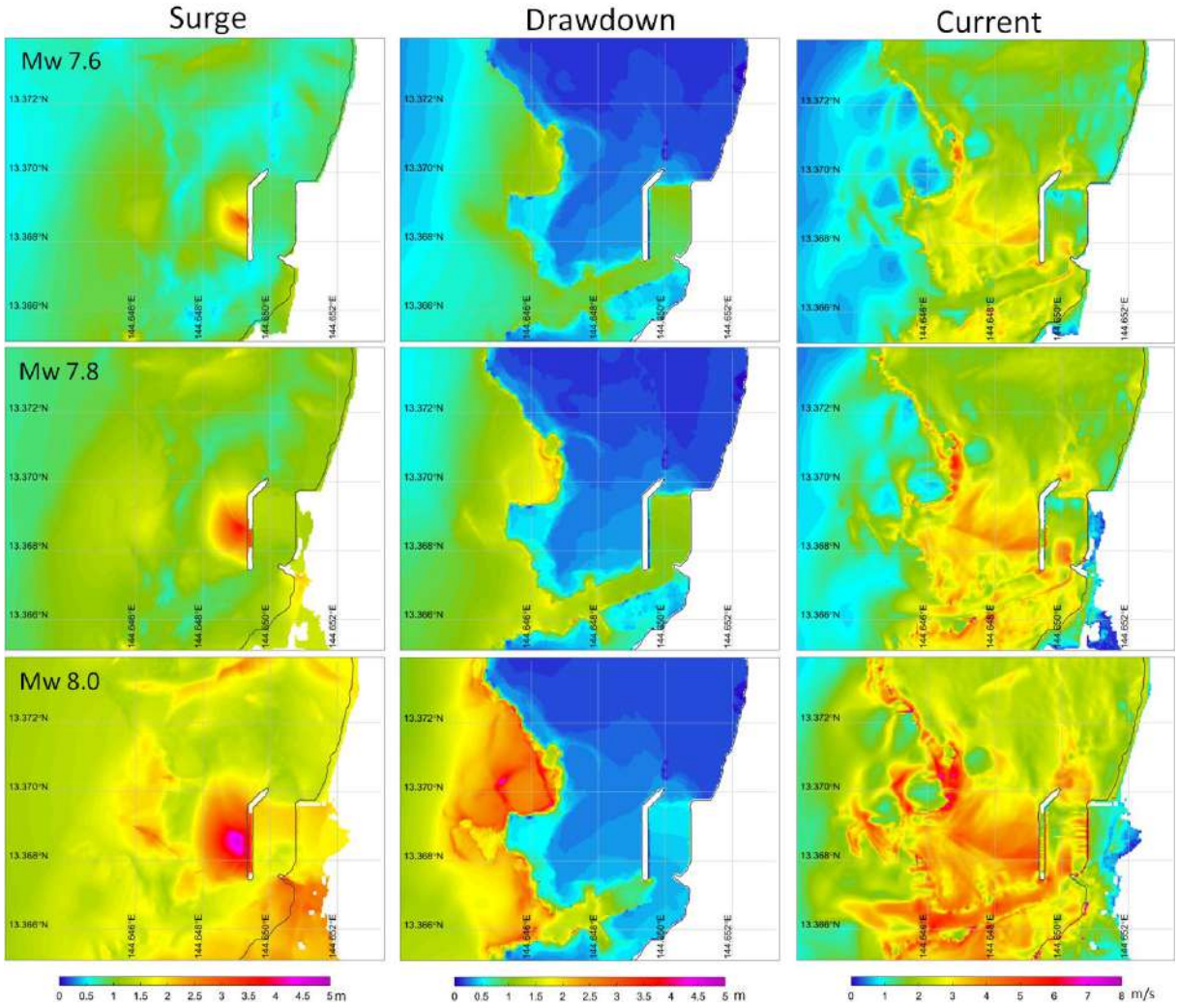

Figure 4. Surge, drawdown, and current at Agat Marina from the Mw 7.6, 7.8, and 8.0 Mariana Trench earthquake scenarios. White areas indicate dry land including the marina parking lot.

The Nankai subduction zone is located 2300 km from Guam with a tsunami travel time of 3 hours. Damaging tsunamis to Guam would involve larger earthquakes at the distant source. Figure 5 shows the surge, drawdown, and current from tsunamis generated by Mw 8.3, 8.5, and 8.7 earthquakes. The selected events demonstrate the impact as the surge transitions from advisory to warning levels. In contrast to local Mariana events, the longer waves associated with the larger rupture area and smaller dip angle are excited to a lesser extent by the steep slope and narrow shelf off Agat. The variation of the near-shore wave amplitude is more gradual. The Mw 8.3 event, which has less than 1 m wave amplitude on the open coast, is at the advisory level. Both the surge and drawdown are slightly over 1 m in the marina and the current is up to 2.7 m/s at its entrance. The Mw 8.5 event is at the warning level and a surge of 1.4 m floods the marina parking lot. The drawdown and current increase slightly to 1.2 m and 2.9 m/s in the marina. The Mw 8.7 event produces very similar drawdown and current albeit with a slightly larger surge of 1.5 m at the marina.

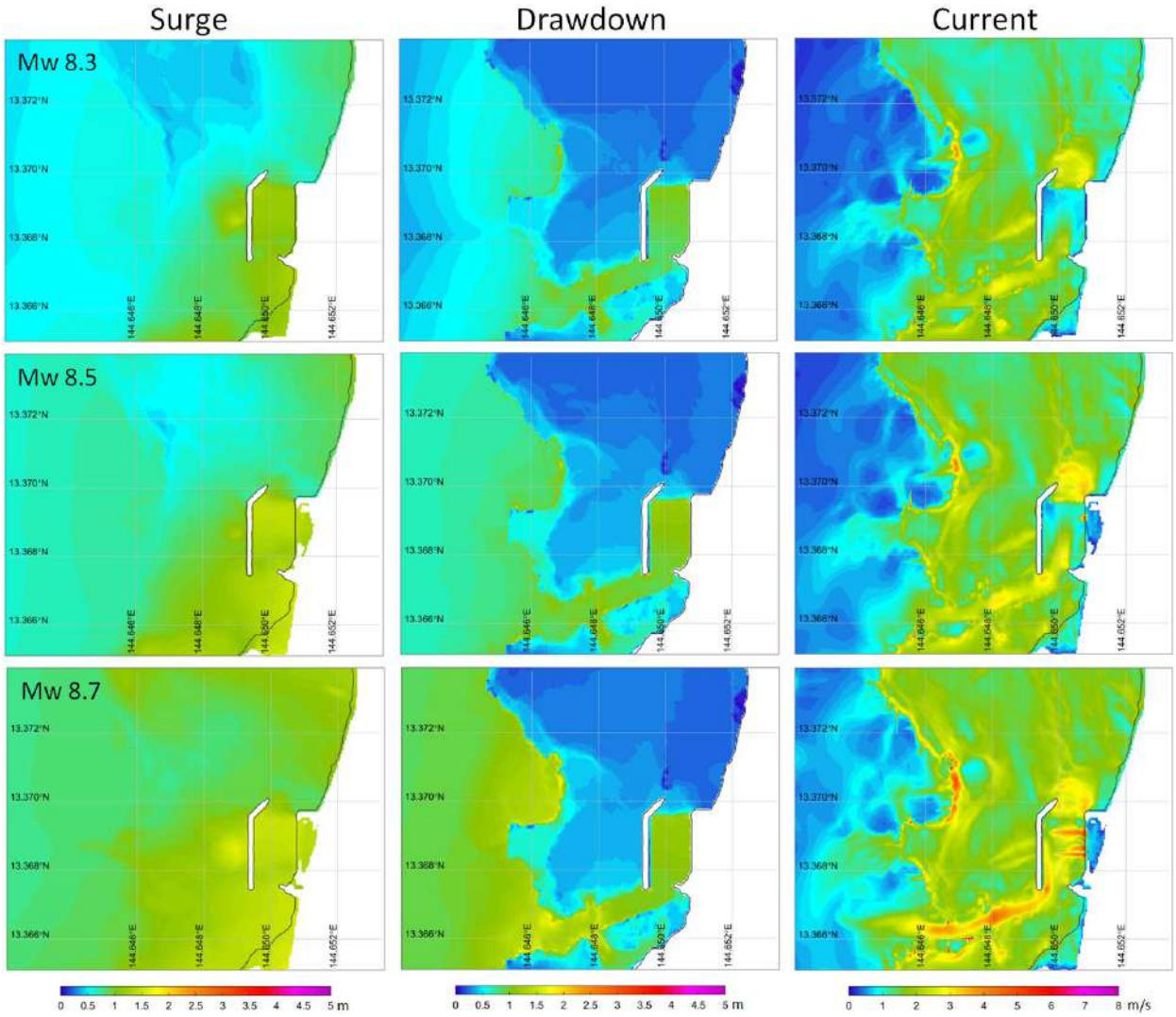

Figure 5. Surge, drawdown, and current at Agat Marina from the Mw 8.3, 8.5, and 8.7 Nankai Trough earthquake scenarios. White areas indicate dry land including the marina parking lot.

Tsunamis from the Philippine source have the most direct approach to the Agat shore. The travel time of 2.5 hr is shorter compared to Nankai trough events due to the slightly shorter distance of 2000 km and deeper water in the East Philippine Sea. The large dip angle of the fault and the deeper water at the trench also enhance the energy of the tsunami generated by seafloor deformation while reducing the wave period. Figure 6 illustrates the transition from advisory to warning-level tsunamis generated by Mw 8.0, 8.2, and 8.4 earthquakes. In comparison to the Nankai trough events, the shorter waves from the Philippine sources generate more localized excitations over the shallow reefs similar to local Mariana events. In the Mw 8.0 scenario, the tsunami generates 1.1 m of drawdown and 2.6 m/s of current in the marina. The flow conditions might be dangerous to boats and moorings even without inundation of the marina parking lot. The surge, drawdown, and current increase to 1.5 m, 1.3 m, and 4.1m/s for the Mw 8.2 warning threshold event, when evacuation is deemed necessary.

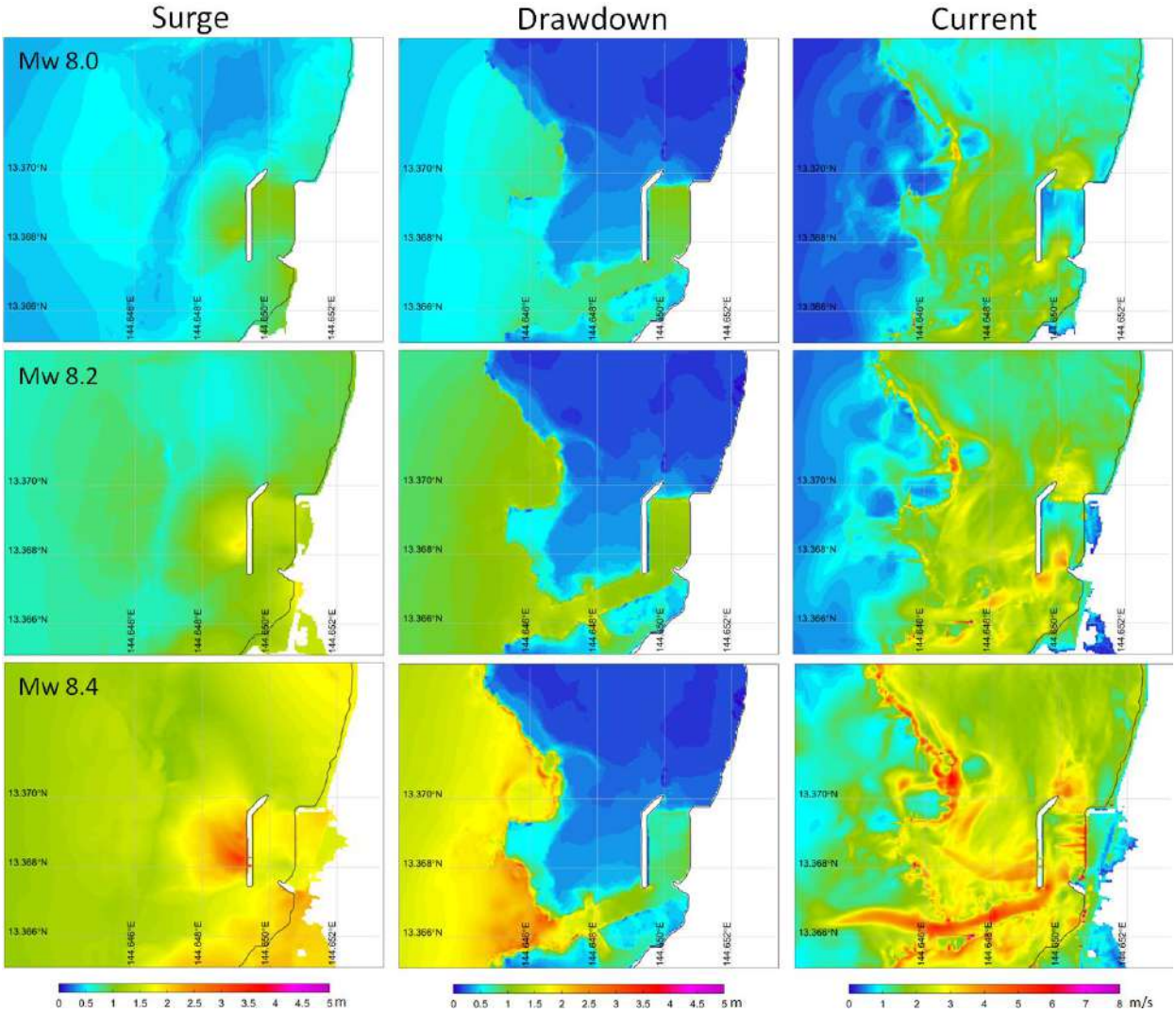

Figure 6. Surge, drawdown, and current at Agat Marina from the *Mw* 8.0, 8.2, and 8.4 Philippine Trench earthquake scenarios. White areas indicate dry land including the marina parking lot.

The New Guinea subduction zone is 1800 km from Guam with a tsunami travel time of 2.4 hr. The small dip angle of the fault plane is ineffective in generating seafloor uplift, which is the primary source of tsunami energy from earthquake rupture. The wave period tends to be long and increases with the earthquake magnitude. The resulting tsunamis reaching Guam also have their amplitude reduced by diversion of the energy through Yap Trench and Mariana Trench. Any significant tsunami events from the New Guinea source will involve large earthquake magnitudes. Figure 7 shows the surge, drawdown, and current generated by Mw 8.4, 8.6, and 8.8 earthquakes. The oscillation pattern is close to that from the Nankai source, but with more gradual variation of wave amplitude in the nearshore area. The surge, drawdown, and current reach 1.4 m, 1.1 m, and 4.2 m/s in the marina for the Mw 8.8 event. This is the preferred maximum at the New Guinea subduction zone (Berryman et al., 2015), but the potential impacts are close to the threshold for warning.

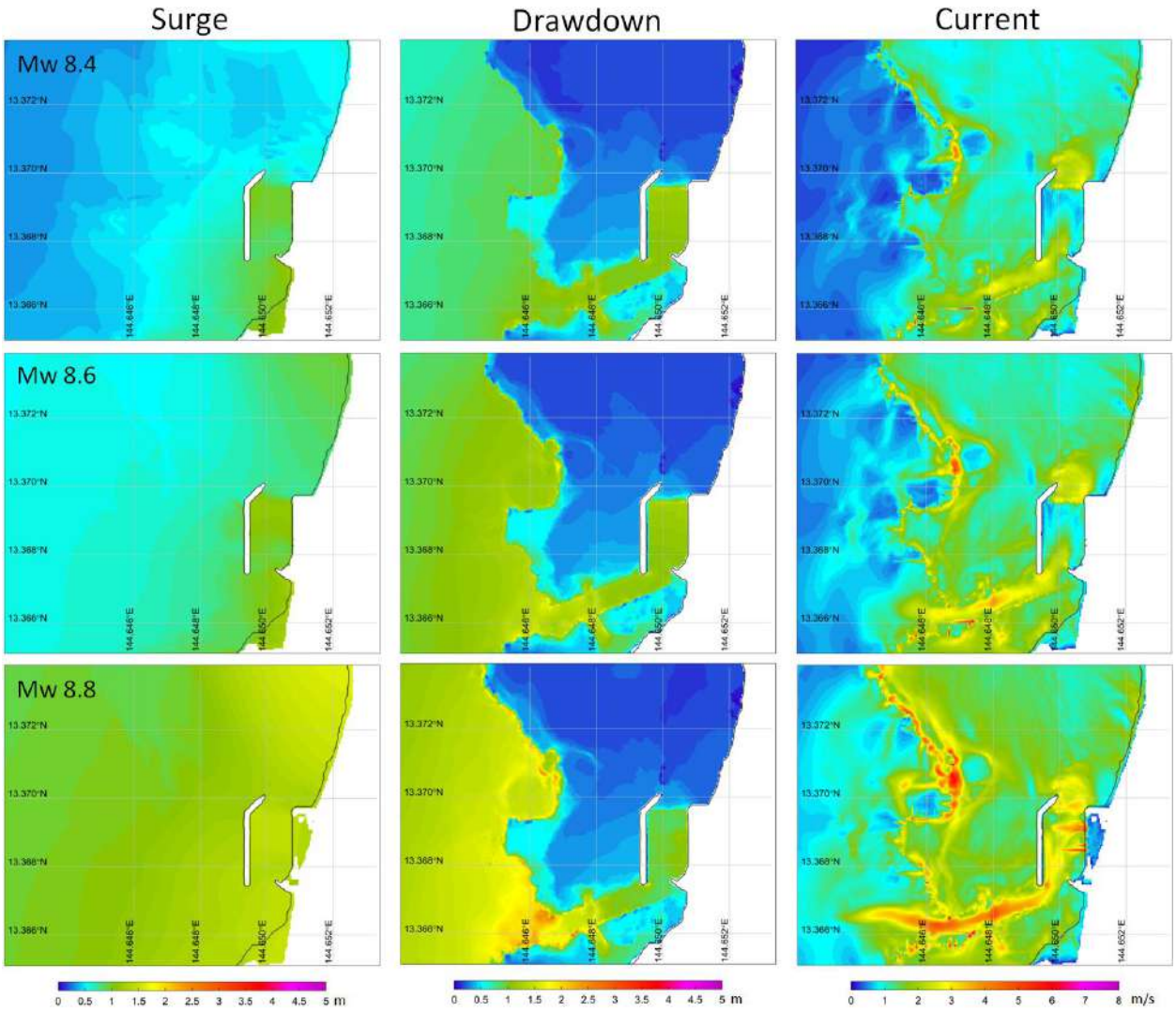

Figure 7. Surge, drawdown, and current at Agat Marina from the *Mw* 8.4, 8.6, and 8.8 New Guinea earthquake scenarios. White areas indicate dry land including the marina parking lot.

3.2 Probable Maximum Scenarios

The USCG District 14 emergency response plan calls for evacuation of vessels from harbors for all warning-level tsunamis. Berryman et al. (2015) provides the preferred maximum earthquakes at the four most critical subduction zones to Guam from which the modeled tsunamis can be sued to determine how far offshore vessels need to be evacuated to. However, it is necessary to consider locally-generated and far-field tsunamis separately in the response plan due to the difference in arrival time.

Figure 8 shows the surge, drawdown, and current for the preferred, maximum Mariana scenario with Mw 8.3 from Berryman et al. (2015). The local tsunami severely impacts the east and north-facing shores of Guam with considerable flooding into low-lying river valleys. The initial wave arrives at Agat Marina 10 min after the earthquake and reaches its peak 6 min afterward. The short timeframe precludes any warning instructions from being issued or implemented and a strong earthquake will be a sign of an imminent tsunami. In addition, the currents can be treacherous in the 500 m long channel posing danger to vessels in transit. It is not advisable to evaluate vessels from Agat Marina in the event of a local tsunami.

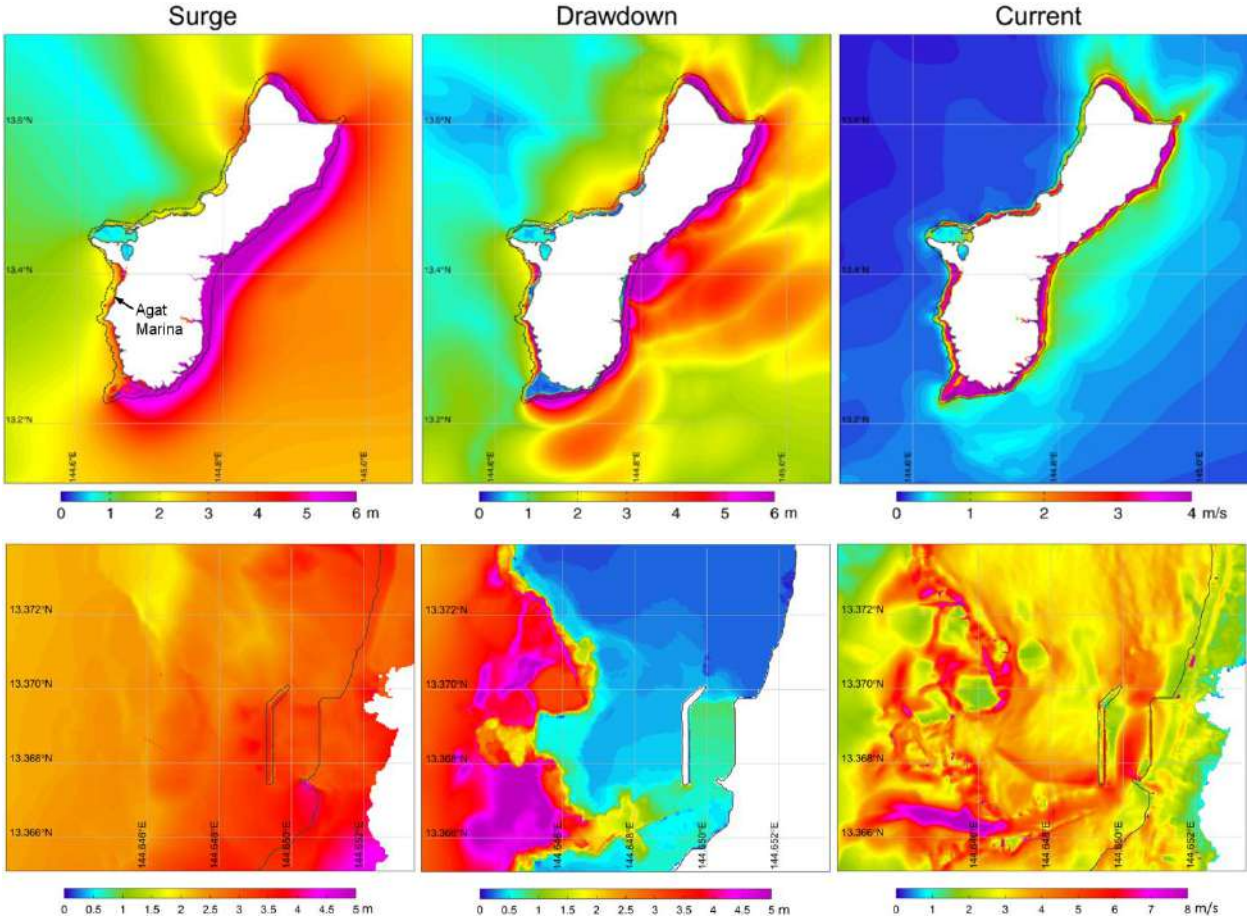

Figure 8. Surge, drawdown, and current from tsunamis generated by the preferred maximum earthquake at Mariana Trench. Black solid lines denote the coastlines, and in the upper panels, the black dashed lines indicate the 100-m depth contour delineating the approximate extent of the insular shelf.

A tsunami from the Nankai, Philippine, and New Guinea sources has at least 2.4 hours of travel time to Guam. If a tsunami warning is issued in time, most of the vessels might be able to evacuate from their docks to designated areas with reduced wave action. Among the three probable maximum far-field tsunamis, the Mw 8.5 Philippine scenario has the most severe impact overall. The results are aggregated with those from the Mw 8.7 Nankai and 8.8 New Guinea scenarios to account for localized responses due to directivity and resonance of the tsunamis. Figure 9 shows the aggregated surge, drawdown, and current. There are potential refuge areas 8 km northwest of Apra Harbor with surge and drawdown as low as 0.8 and 0.7 m with negligible currents. The central portion of outer Apra Harbor, which has less than 0.8 m of surge and drawdown and 0.4 m/s of current, can also serve as a refuge for evacuated vessels from Agat Marina.

The 100 m depth contour, which is the upper limit for demarcation of offshore refuge areas by NTHMP partner states and territories, appears to be insufficient for Guam. The model results confirms that the refuge areas are more appropriately delineated by distance from shore due to the steep insular slope and concentration of energy nearshore.

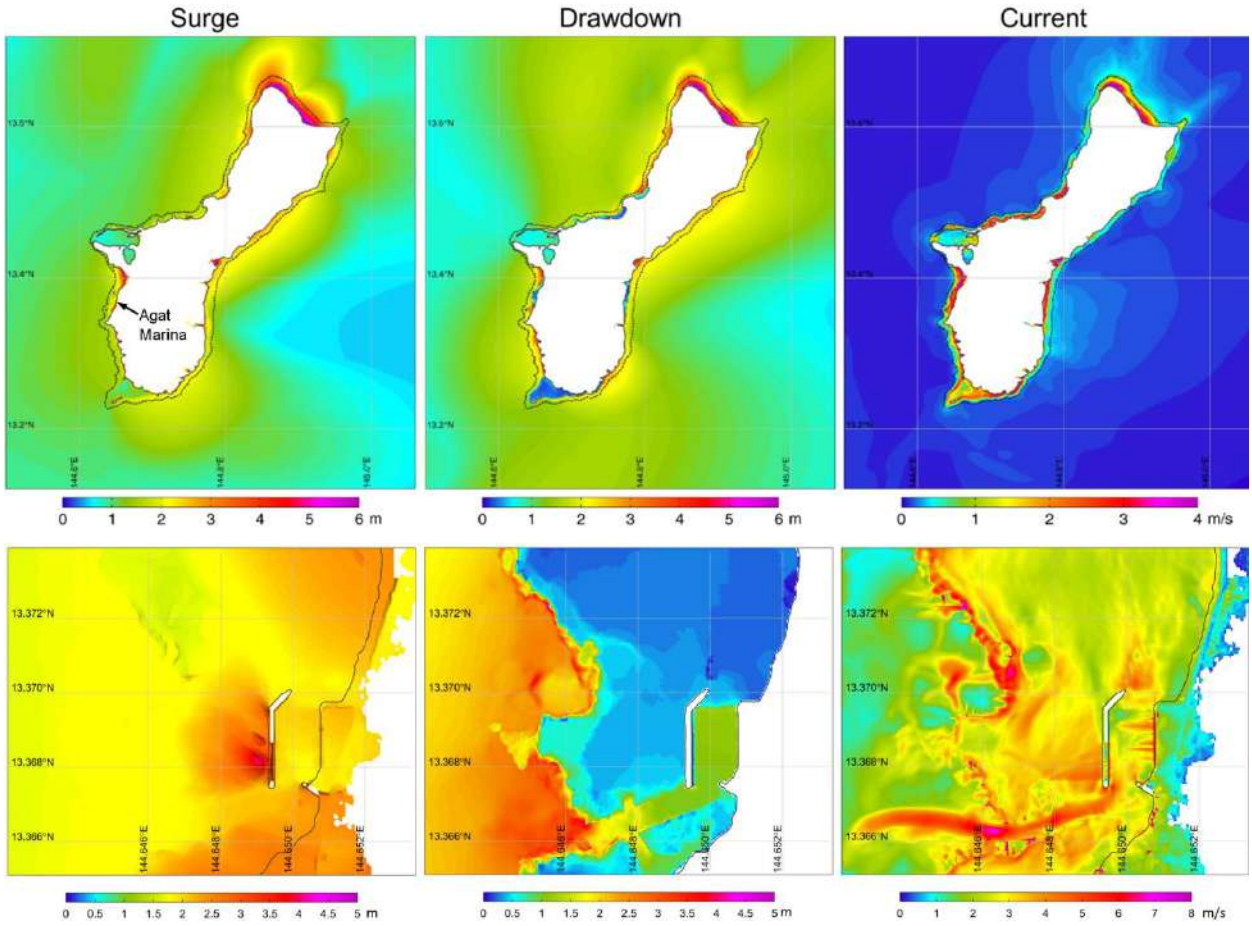

Figure 9. Aggregated surge, drawdown, and current from tsunamis generated by the preferred maximum earthquakes at Philippine Trench, Nankai Trough, and New Guinea Trench. Black solid lines denote the coastlines, and in the upper panels, the black dashed lines indicate the 100-m depth contour delineating the approximate extent of the insular shelf.

4. Summary Tables

The modeling work has produced a large volume of temporal-spatial data for determination of the surge, drawdown, and current at Agat Marina from tsunamis generated by potential Mariana, Nankai, Philippine, and New Guinea earthquakes. These scenarios cover ranges of earthquake magnitude up to the preferred maxima suggested by Berryman et al. (2015). We identified three critical areas in consultation with Guam Department of Homeland Security for compilation of a data summary. These are Agat Marina, Agat Channel, and Nimitz Beach (including access channels to the shore), as shown in Figure 10. Tables 3 through 6 list the maximum surge, drawdown, and current in the three areas as functions of earthquake magnitude for the Mariana, Nankai, Philippine, and New Guinea sources. The modeling work is based on the mean-sea level (MSL) such that the tabulated surge and drawdown will reference the tide level during an actual event.

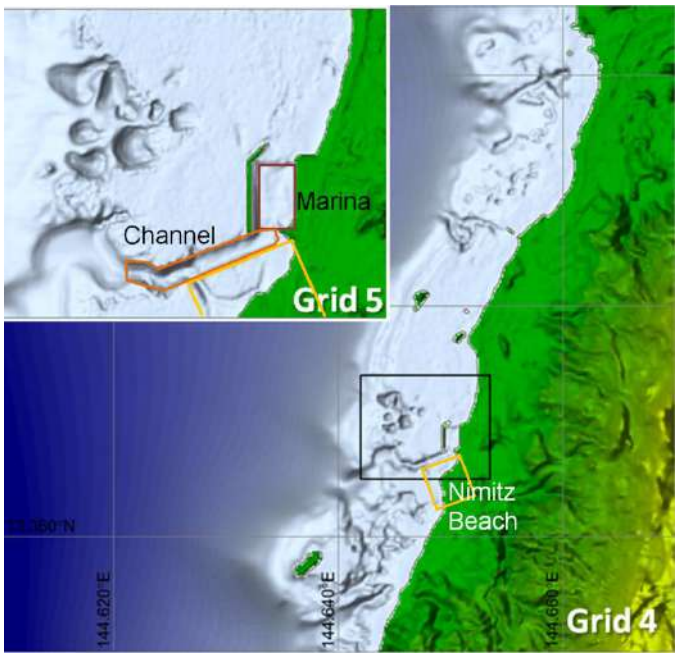

Figure 10. Areas for compilation of summary tables.

The dynamic response of the coast water is multi-modal due to broad-band excitation of the oscillation modes associated with the morphology of the Mariana Island chain. The tables also include periods of the two most energetic oscillation components in each area. There is a general upward trend of the surge, drawdown, current, and the respective oscillation periods with earthquake magnitude. The variation, however, is not necessarily continuous due to transition from one oscillation mode to another as the tsunami wave period increases with larger earthquakes. In addition, the drawdown in the marina tends to stabilize or decrease for the large events, when overtopping of the breakwater and marina provides additional floodwater at the shore. As the maximum surface elevation and current are driven by distinct oscillation modes at separate locations within each area of interest, their dominant periods can be quite different. In contrast to earlier modeling work for Guam, the flows in the three areas of interest here are interconnected and driven by the same mechanisms with similar dominant wave periods. These summary tables of potential surge, drawdown, and current (in feet and knots) allow quick assessment of the situation and formulation of a course of action during the initial stage of a tsunami. The data can support informed decisions on closure of facilities in an advisory event, when evacuation of coastal residents is not mandatory.

The maritime hazard maps and data products presented in this and earlier progress reports compliment the inundation maps developed by Uslu et al. (2010) of NOAA PMEL in managing and mitigating the tsunami hazards in Guam.

Table 3. Maximum surge, drawdown, and current from Mariana Trench tsunamis

Mariana Mw	Agat Marina				
	Surge (ft)	Drawdown (ft)	Period (min)	Current (knot)	Period (min)
7.6	3.1	3.5	8, 10	6.7	7, 10
7.7	3.7	4.3	8, 10	7.3	8, 10
7.8	4.5	3.9	8, 10	8.7	8, 10
7.9	5.7	2.7	8, 10	7.9	8, 10
8.0	6.7	1.7	8, 10	9.5	8, 10
8.1	7.9	2.2	8, 10	11.2	8, 10
8.2	9.4	2.5	8, 10	12.3	8, 10
8.3	10.9	2.8	8, 10	12.6	8, 10
	Agat Channel				
	Surge (ft)	Drawdown (ft)	Period (min)	Current (knot)	Period (min)
7.6	2.3	3.6	8, 10	6.3	7, 10
7.7	2.6	4.2	8, 10	6.6	8, 10
7.8	3.1	4.3	8, 10	7.0	8, 10
7.9	4.3	5.3	8, 10	9.6	8, 10
8.0	5.5	5.9	8, 10	10.2	8, 10
8.1	7.9	6.1	8, 10	10.6	8, 10
8.2	9.6	6.4	8, 10	11.1	8, 10
8.3	12.4	6.4	8, 10	11.5	8, 10
	Nimitz Beach				
	Surge (ft)	Drawdown (ft)	Period (min)	Current (knot)	Period (min)
7.6	4.5	4.3	8, 10	6.9	7, 10
7.7	4.6	4.3	8, 10	7.8	8, 10
7.8	5.4	5.0	8, 10	9.5	8, 10
7.9	7.3	5.2	8, 10	10.2	8, 10
8.0	8.5	5.6	8, 10	10.7	8, 10
8.1	8.7	6.1	8, 10	11.3	8, 10
8.2	10.6	6.2	8, 10	11.5	8, 10
8.3	12.8	6.7	8, 10	12.5	8, 10

Table 4. Maximum surge, drawdown, and current from Nankai Trough tsunamis

Nankai Mw	Agat Marina				
	Surge (ft)	Drawdown (ft)	Period (min)	Current (knot)	Period (min)
8.1	2.8	3.1	8, 9	4.1	8, 9
8.2	3.3	3.3	7, 9	4.5	8, 15
8.3	4.0	3.4	7, 15	4.8	7, 15
8.4	4.5	3.5	7, 15	5.3	7, 15
8.5	4.6	3.8	7, 15	5.7	7, 17
8.6	4.5	3.9	7, 17	5.4	7, 17
8.7	4.8	3.8	7, 17	8.2	7, 19

	Agat Channel				
	Surge (ft)	Drawdown (ft)	Period (min)	Current (knot)	Period (min)
8.1	2.6	2.8	8, 9	4.1	8, 9
8.2	3.2	3.1	7, 9	5.0	8, 15
8.3	3.8	3.3	7, 15	5.6	7, 15
8.4	4.3	3.3	7, 15	5.9	7, 15
8.5	4.5	3.6	7, 15	5.9	7, 17
8.6	4.5	3.9	7, 17	6.2	7, 17
8.7	4.7	5.0	7, 17	8.7	7, 17
	Nimitz Beach				
	Surge (ft)	Drawdown (ft)	Period (min)	Current (knot)	Period (min)
8.1	2.8	3.2	8, 9	4.7	8, 9
8.2	3.4	3.6	7, 9	5.7	8, 15
8.3	3.9	4.2	7, 15	6.0	7, 15
8.4	4.6	4.2	7, 15	6.0	7, 15
8.5	4.9	4.0	7, 15	5.9	7, 17
8.6	4.8	4.3	7, 17	5.9	7, 17
8.7	4.9	5.1	7, 17	6.5	6, 17

Table 5. Maximum surge, drawdown, and current from Philippine Trench tsunamis

Philippine Mw	Agat Marina				
	Surge (ft)	Drawdown (ft)	Period (min)	Current (knot)	Period (min)
7.9	2.9	2.7	7, 9	4.5	7, 9
8.0	3.5	3.5	7, 9	5.6	7, 9
8.1	4.1	3.8	7, 9	6.4	7, 9
8.2	4.8	3.9	7, 9	8.0	7, 9
8.3	5.4	4.0	7, 9	9.6	7, 9
8.4	6.2	3.0	7, 9	8.0	7, 9
8.5	7.1	1.2	7, 9	7.8	7, 9
	Agat Channel				
	Surge (ft)	Drawdown (ft)	Period (min)	Current (knot)	Period (min)
7.9	2.1	2.2	7, 9	4.5	7, 9
8.0	2.8	3.1	7, 9	5.6	7, 9
8.1	3.5	3.7	7, 9	6.2	7, 9
8.2	4.1	4.7	7, 9	7.1	7, 9
8.3	4.9	5.3	7, 9	8.5	7, 9
8.4	6.2	6.4	7, 9	11.3	7, 9
8.5	7.4	6.5	7, 9	11.9	7, 9
	Nimitz Beach				
	Surge (ft)	Drawdown (ft)	Period (min)	Current (knot)	Period (min)
7.9	2.4	2.4	7, 9	3.4	7, 9
8.0	3.2	3.2	7, 9	4.8	7, 9

8.1	4.1	4.3	7, 9	5.7	7, 9
8.2	4.9	5.2	7, 9	6.3	7, 9
8.3	5.8	5.8	7, 9	6.6	7, 9
8.4	6.8	6.1	7, 9	8.1	7, 9
8.5	8.1	6.5	7, 9	9.2	7, 9

Table 6. Maximum surge, drawdown, and current from New Guinea Trench tsunamis

New Guinea Mw	Agat Marina				
	Surge (ft)	Drawdown (ft)	Period (min)	Current (knot)	Period (min)
8.2	3.1	3.2	8, 9	4.5	7, 8
8.3	3.2	3.7	8, 9	4.7	7, 8
8.4	3.3	4.0	8, 9	4.9	7, 8
8.5	3.4	4.0	7, 8	5.2	7, 8
8.6	3.8	4.0	7, 8	5.2	7, 8
8.7	3.7	4.0	7, 10	5.8	7, 8
8.8	4.8	3.6	7, 10	5.8	7, 10
	Agat Channel				
	Surge (ft)	Drawdown (ft)	Period (min)	Current (knot)	Period (min)
8.2	3.0	3.0	8, 9	4.9	8, 9
8.3	3.1	3.6	8, 9	5.3	8, 9
8.4	3.3	4.1	8, 9	5.8	7, 8
8.5	3.3	4.7	7, 8	6.8	7, 8
8.6	3.5	4.9	7, 8	7.4	7, 8
8.7	3.5	4.9	7, 10	8.1	7, 8
8.8	4.6	5.7	7, 10	9.7	7, 10
	Nimitz Beach				
	Surge (ft)	Drawdown (ft)	Period (min)	Current (knot)	Period (min)
8.2	3.2	3.0	8, 9	4.3	7, 8
8.3	3.4	3.8	8, 9	5.1	7, 8
8.4	3.5	5.2	8, 9	5.8	7, 8
8.5	3.6	4.9	7, 8	6.1	7, 8
8.6	3.8	5.2	7, 8	6.3	7, 8
8.7	3.7	5.7	7, 10	6.5	7, 10
8.8	4.7	6.3	7, 10	6.7	7, 10

References

Ando, M. (1975). Source mechanisms and tectonic significance of historical earthquakes along the Nankai Trough, Japan. *Tectonophysics*, 27(2), 119–140.

Bai, Y., Yamazaki, Y., and Cheung, K.F. (2015). NEOWAVE. Proceedings and Results of the 2015 National Tsunami Hazard Mitigation Program Model Benchmarking Workshop, Portland, Oregon, 165-177.

Bai, Y. Yamazaki, Y., and Cheung, K.F. (2018). Amplification of tsunami drawdown and runup in the Hawaiian Islands by near-trench slip of mega Aleutian earthquakes. *Ocean Modelling*, 124, 61-74.

Berryman, K., Wallace, L., Hayes, G., Bird, P., Wang, K., Basili, R., Lay, T., Pagani, M., Stein, R., Sagiya, T., Rubin, C., Barreintos, S., Kreemer, C., Litchfield, N., Stirling, M., Gledhill, K., Costa, C. (2015). The GEM Faulted Earth Subduction Characterization Project, Version 2.0, available from http://www.nexus.globalquakemodel.org/gem-faulted-earth/posts.

Bretschneider, C.L., Krock, H.J., Nakazaki, E., and Casciano, F.M. (1986). Roughness of Typical Hawaiian Terrain for Tsunami Run-up Calculations: A User's Manual. J.K.K. Look Laboratory Report, University of Hawaii, Honolulu, Hawaii.

Cheung, K.F., Bai, Y., and Yamazaki, Y. (2013). Surges around the Hawaiian Islands from the 2011 Tohoku Tsunami. *Journal of Geophysical Research: Oceans*, 118(10), 5703-5719.

Gica, E., Spillane, M.C., Titov, V.V., Chamberlin, C.D., and Newman, J.C. (2008). Development of the Forecast Propagation Database for NOAA's Short Term Inundation Forecast for Tsunamis (SIFT). NOAA Technical Memorandum OAR PMEL-139, Pacific Marine Environmental Laboratory Seattle, WA, 89 pp.

Kanamori, H. (1977). The energy release in great earthquake. *Journal of Geophysical Research*, 82 (20), 2981–2987.

Lay, T., Ye, L., Bai, Y., Cheung, K.F., Kanamori, H., Freymueller, J., Steblov, G.M., and Kogan, M.G. (2017). Rupture along 400 km of the Bering Fracture Zone in the Komandorsky Islands Earthquake (Mw 7.8) of 17 July 2017. *Geophysical Research Letters*, 44(24), 12,161–12,169.

Li, L. and Cheung, K.F. (2019). Numerical dispersion in non-hydrostatic modeling of long-wave propagation. *Ocean Modelling*, 138, 68-87.

Okada, Y. (1985), Surface deformation due to shear and tensile faults in a half space. *Bulletin of the Seismological Society of America*, 75(4), 1135-1154.

Roeber, V., Yamazaki, Y., and Cheung, K.F. (2010). Resonance and impact of the 2009 Samoa tsunami around Tutuila, American Samoa. *Geophysical Research Letters*, 37(21), L21604, Doi: 10.1029/2010GL044419.

Ross, S.L., Jones, L.M., Miller, K, Porter, K.A., Wein, A., Wilson, R.I., Bahng, B., Barberopoulou, A., Borrero, J.C., Brosnan, D.M., Bwarie, J.T., Geist, E.L., Johnson, L.A., Kirby, S.H., Knight, W.R., Long, K., Lynett, P., Mortensen, C.E., Nicolsky, D.J., Perry, S.C., Plumlee, G.S., Real, C.R., Ryan, K., Suleimani, E., Thio, H., Titov, V.V., Whitmore, P.M. and Wood, N.J. (2013). SAFRR (Science Application for Risk Reduction) Tsunami Scenario—Executive Summary and Introduction: U.S. Geological Survey Open-File Report 2013–1170–A, *in* Ross, S.L., and Jones, L.M., eds., The SAFRR (Science Application for Risk Reduction) Tsunami Scenario: U.S. Geological Survey Open-File Report 2013–1170, 17 p., http://pubs.usgs.gov/of/2013/1170/a/.

Uslu, B., Titov, V.V., Eble, M. and Chamberlin, C.D. (2010). Tsunami Hazard Assessment Specifal Series: Vol. 1 Guam. NOAA Pacific Marine Environmental Laboratory, OAR Special Report, Seattle, Washington.

Yamazaki, Y., Cheung, K.F., and Kowalik, Z. (2011). Depth-integrated, non-hydrostatic model with grid nesting for tsunami generation, propagation, and run-up. *International Journal for Numerical Method in Fluids*, 67(12), 2081-2107.

Yamazaki, Y., K.F. Cheung, Z. Kowalik, G. Pawlak, and T. Lay (2012). NEOWAVE. Proceedings and Results of the 2011 National Tsunami Hazard Mitigation Program Model Benchmarking Workshop, Galveston, Texas, pp. 239-302.

Yamazaki, Y., Kowalik, Z., and Cheung, K.F. (2009). Depth-integrated, non-hydrostatic model for wave breaking and runup. *International Journal for Numerical Method in Fluids,* 61(5), 473-497.

Ye, L., Lay, T., Kanamori, H., and Rivera, L. (2016). Rupture characteristics of major and great ($M_w \geq 7.0$) megathrust earthquakes from 1990 to 2015: 1. Source parameter scaling relationships, *Journal of Geophysical Research: Solid Earth,* 121(2), 826–844.

Ye, L., Lay, T., Kanamori, H., and Rivera, L. (2016). Rupture characteristics of major and great ($M_w \geq 7.0$) megathrust earthquakes from 1990 to 2015: 2. Depth dependence. *Journal of Geophysical Research: Solid Earth,* 121(2), 845–863.